Functional and Structural Characterization of DR_0079 from *Deinococcus radiodurans*, a Novel Nudix Hydrolase with a Preference for Cytosine (Deoxy)ribonucleoside 5′-Di- and Triphosphates†

Garry W. Buchko,*,‡ Olga Litvinova,§ Howard Robinson,‖ Alexander F. Yakunin,§ and Michael A. Kennedy‡,⊥

Biological Sciences Division, Pacific Northwest National Laboratory, Richland, Washington 99352, Banting and Best Department of Medical Research, University of Toronto, Toronto, Ontario, Canada M5G 1L6, and Biology Department, Brookhaven National Laboratory, Upton, New York 11973

Received January 18, 2008; Revised Manuscript Received April 21, 2008

ABSTRACT: The genome of the extremely radiation resistant bacterium *Deinococcus radiodurans* encodes 21 Nudix hydrolases, of which only two have been characterized in detail. Here we report the activity and crystal structure for DR_0079, the first Nudix hydrolase observed to have a marked preference for cytosine ribonucleoside 5′-diphosphate (CDP) and cytosine ribonucleoside 5′-triphosphate (CTP). After CDP and CTP, the next most preferred substrates for DR_0079, with a relative activity of <50%, were the corresponding deoxyribose nucleotides, dCDP and dCTP. Hydrolase activity at the site of the phosphodiester bond was corroborated using ^{31}P NMR spectroscopy to follow the phosphorus resonances for three substrates, CDP, IDP, and CTP, and their hydrolysis products, CMP + P_i, IMP + P_i, and CMP + PP_i, respectively. Nucleophilic substitution at the β-phosphorus of CDP and CTP was established, using ^{31}P NMR spectroscopy, by the appearance of an upfield-shifted P_i resonance and line-broadened PP_i resonance, respectively, when the hydrolysis was performed in 40% $H_2{}^{18}O$-enriched water. The optimal activity for CDP was at pH 9.0−9.5 with the reaction requiring divalent metal cation ($Mg^{2+} > Mn^{2+} > Co^{2+}$). The biochemical data are discussed with reference to the crystal structure for DR_0079 that was determined in the metal-free form at 1.9 Å resolution. The protein contains nine β-strands, three α-helices, and two 3_{10}-helices organized into three subdomains: an N-terminal β-sheet, a central Nudix core, and a C-terminal helix−turn−helix motif. As observed for all known structures of Nudix hydrolases, the α-helix of the "Nudix box" is one of two helices that sandwich a "four-strand" mixed β-sheet. To identify residues potentially involved in metal and substrate binding, NMR chemical shift mapping experiments were performed on ^{15}N-labeled DR_0079 with the paramagnetic divalent cation Co^{2+} and the nonhydrolyzable substrate thymidine 5′-*O*-(α,β-methylenediphosphate) and the results mapped onto the crystal structure.

Nudix hydrolases are widely distributed among species, having been found in the genomes of all three kingdoms and in organisms as diverse as viruses and humans (*1*). They are identified by a highly conserved sequence of amino acids, $GX_5EX_7REUXEEXGU$ (where U is an aliphatic and hydrophobic amino acid and X is any amino acid). This conserved sequence, called the "Nudix box", forms part of the substrate-binding and catalytic site for the hydrolysis of nucleoside diphosphates linked to some other moiety, x, from whence the acronym Nudix arose (*2, 3*). The glutamic acid residues in the core of the Nudix box, REUXEE, play a critical role in binding one to three divalent cations. At least one cation is essential for hydrolase activity, and under physiological conditions, the most relevant cation is likely Mg^{2+} (*3*). Nudix substrates include capped mRNA (*4*), dinucleotide coenzymes, nucleotide sugars, nucleotide alcohols, dinucleotide polyphosphates, and both canonical and oxidized (deoxy)-ribonucleoside triphosphates (NTPs) (*5*). Non-nucleotide Nudix substrates, such as thiamine pyrophosphate (*6*) and diphosphoinositol polyphosphates (*7*), have also been identified. By hydrolyzing such compounds, the Nudix proteins effect the elimination of potentially toxic endogenous nucleotide metabolites from the cell and regulate the intracellular concentration of nucleotide cofactors and signaling molecules (*3, 8, 9*). For example, the prototypical member of the Nudix superfamily is the *Escherichia coli* MutT protein.

† The research was performed in the Environmental Molecular Sciences Laboratory [a national scientific user facility sponsored by the U.S. Department of Energy (DOE) Biological and Environmental Research] located at Pacific Northwest National Laboratory and operated for DOE by Battelle, as well as in the Ontario Centre for Structural and Functional Proteomics at the University of Toronto. Support for beamline X29A at the National Synchrotron Light Source comes principally from the Office of Biological and Environmental Research and of Basic Energy Sciences of the DOE, and from the National Center for Research Resources of the National Institutes of Health (NIH). This work was funded by grants from the DOE, Office of Biological Energy Research (Contract DE-AC03-76SF00098), Genome Canada (through the Ontario Genomics Institute), the Ontario Research and Development Challenge Fund, and the Protein Structure Initiative of the National Institutes of Health (Midwest Center for Structural Genomics, NIH Grant GM 62414).

* To whom correspondence should be addressed. Telephone: (509) 371-6543. Fax: (509) 371-6546. E-mail: garry.buchko@pnl.gov.
‡ Pacific Northwest National Laboratory.
§ University of Toronto.
‖ Brookhaven National Laboratory.
⊥ Current address: Department of Chemistry and Biochemistry, Miami University, Oxford, OH 45056.

10.1021/bi800099d CCC: $40.75
Published on Web 05/31/2008

MutT preferably hydrolyzes 7,8-dihydro-8-oxoguanosine triphosphate (8-oxo-dGTP),[1] a promutagenic compound generated during normal cellular metabolism and upon exposure to oxidative stress (*10*), into nonmutagenic nucleoside monophosphate and inorganic pyrophosphate (*3, 11*) by catalyzing the nucleophilic substitution by H_2O at the β-phosphorus (*12*).

Structures have been determined for a number of the proteins in the Nudix superfamily using both NMR-based and crystallographic methods, including *E. coli* MutT (nucleoside triphosphate pyrophosphohydroylase) (*13*), *Caenorhabditis elegans* and *Lipinus angustifolius* Ap_4A hydrolase (*14, 15*), *E. coli*, *Mycobacterium tuberculosis,* and *Homo sapiens* ADP-ribose pyrophosphatase (*16–18*), *E. coli* dihydroneopterin triphosphatase (*19*), and *Deinococcus radiodurans* coenzyme A pyrophosphatase (*20*). These structures have also been determined in a variety of states, such as with and without bound divalent cation and/or substrate. While the characterized Nudix proteins hydrolyze different substrates, they all conserve the Nudix box located on one of two α-helices that sandwich a central mixed β-sheet core (*1, 21*).

Recently, a new group of substrates for some members of the Nudix hydrolase superfamily has been identified. Fischer et al. (*22*) first reported that the *D. radiodurans* protein DR_0975 had a marked degree of specificity for ribonucleoside and deoxyribonucleoside 5′-diphosphates [(d)NDPs]. Previously, Nudix hydrolase activity toward (d)NDPs had only been reported for one Nudix hydrolase, human NUDT5 ADP-sugar pyrophosphatase (*23*). Subsequently, activity toward (d)NDPs was reported for the *ytkD* gene product from *Bacillus subtilis* (*8*), and Orf17 (NtpA) (*24*) and orf153 (*25*) from *E. coli*. Indeed, *E. coli* MutT itself has recently been shown to be active upon 8-oxo-dGDP, although its efficiency on the diphosphate is 4-fold lower than on 8-oxo-dGTP (*26*). The moiety "x" linked to the nucleoside diphosphate is hydrogen or a divalent metal ion, and the hydrolysis products are a nucleoside monophosphate [(d)NMP] and inorganic phosphate (P_i) according to the following reaction:

$$\text{(d)NDP} + H_2O \rightarrow \text{(d)NMP} + \text{phosphate} + H^+$$

Here we report that another *D. radiodurans* Nudix hydrolase, DR_0079, exhibits a marked degree of specificity for ribonucleoside and deoxyribonucleoside 5′-diphosphates. Unlike DR_0975, however, DR_0079 has a preference for cytidine diphosphate (CDP) and cytidine triphosphate (CTP). The solution structure for *D. radiodurans* DR_0079 was previously determined using NMR-based methods (*27*). To complement this solution structure, we report here the first crystal structure of a Nudix hydrolase with a marked specificity for CDP and CTP. Using this new crystal structure, the previously assigned amide resonances in the $^1H-^{15}N$ HSQC spectrum (*28*), and insights obtained from new biochemical studies, chemical shift perturbation experiments (*29, 30*) were performed on ^{15}N-labeled DR_0079 with $CoCl_2$ and the nonhydrolyzable substrate thymidine 5′-*O*-(α,β-methylenediphosphate) (TMP-CP) to map the metal-binding and nucleotide-binding surface, respectively.

EXPERIMENTAL PROCEDURES

All chemicals and enzymes were purchased from Sigma Chemical Co. (St. Louis, MO) except where indicated.

Cloning, Expression, and Purification. The cloning, expression, and purification protocol for ^{15}N-labeled DR_0079 has previously been reported (*28, 31*). The procedure for preparing SeMet-labeled DR_0079 was similar using a protocol that inhibited the methionine biosynthesis pathway (*32*). In brief, this method involved growing the cells at 37 °C to midlog phase ($OD_{600} \sim 0.8$) in M9 minimal medium supplemented with 34 μg/mL kanamycin (RPI Corp., Prospect, IL), 30 μg/mL chloramphenicol, 120 μg/mL $MgSO_4$, 11 μg/mL $CaCl_2$, 10 ng/mL Fe_2Cl_3, 50 μg/mL NaCl, and 4 mg/mL glucose and then lowering the temperature to 25 °C. At this point, lysine (0.1 μg/mL), phenylalanine (0.1 μg/mL), threonine (0.1 μg/mL), isoleucine (0.05 μg/mL), valine (0.05 μg/mL), and selenomethionine (SeMet; 0.06 μg/mL) (Acrös Organics, Geel, Belgium) were added followed by the induction of protein expression ~15 min later with isopropyl β-D-1-thiogalactopyranoside (0.026 μg/mL) (RPI Corp.). Approximately 4−6 h later, the cells were harvested by mild centrifugation and then frozen at −80 °C. From this point forward, the protocol was identical to the previously described protocols except that the last step, gel filtration chromatography on a Superdex75 HiLoad column (GE Healthcare, Piscataway, NJ), used either buffer to grow crystals [100 mM NaCl, 20 mM Tris, and 1 mM dithiothreitol (DTT) (pH 7.1)], to conduct the NMR studies [NMR buffer being 100 mM KCl, 20 mM potassium phosphate, and 2 mM DTT (pH 7.1)], or to conduct enzyme assay experiments [50 mM Hepes and 100 mM NaCl (pH 7.0)].

$CoCl_2$ and TMP-CP Chemical Shift Mapping. Chemical shift mapping experiments (25 °C) with $CoCl_2$ were conducted with DR_0079 following the procedure previously described for $MgCl_2$ and $MnCl_2$ (*27*). Titration experiments were performed in a Shigemi (Tokyo, Japan) tube on a 250 μL sample of 0.6 mM (150 nmol) ^{15}N-labeled DR_0079 in NMR buffer. A stock solution of $CoCl_2$ (50 mM) was added to the protein sample in 1.5 μL (75 nmol) aliquots up to a 2-fold molar excess of the metal ion. Following mild agitation, two-dimensional $^1H-^{15}N$ HSQC spectra, at a ^1H resonance frequency of 900 MHz (Varian Inova-900), were collected after the addition of each aliquot at metal:protein ratios of 0.5, 1.0, and 2.0.

To probe the substrate-binding surface, the hydrolytically stable substrate thymidine-5′-*O*-(α,β-methylenediphosphate), sodium salt (TMP-CP) (Biolog Life Science Institute, Bremen, Germany), was titrated into a solution of DR_0079 containing 100 mM $MgCl_2$ in NMR buffer (*27*). This concentration of Mg^{2+} was chosen because it was the level at which significant chemical shift perturbations were observed in previous titration experiments. TMP-CP (10 mM) was added to 400 μL of DR_0079 solution (0.3 mM, 120 nmol) in 12 μL aliquots (120 nmol) up to a 4-fold molar excess of the substrate. Following mild agitation, two-dimensional $^1H-^{15}N$ HSQC spectra, at a ^1H resonance frequency of 600 MHz (Varian Inova-600), were collected after the addition of each TMP-CP aliquot.

[1] Abbreviations: CDP, cytosine ribonucleoside 5′-diphosphate; CTP, cytosine ribonucleoside 5′-triphosphate; IDP, inosine ribonucleoside 5′-diphosphate; TMP-CP, thymidine-5′-*O*-(α,β-methylenediphosphate); 8-oxo-dGTP, 7,8-dihydro-8-oxoguanosine triphosphate; 8-oxo-dGDP, 7,8-dihydro-8-oxoguanosine diphosphate; IDI, isopentenyl-diphosphate δ-isomerase; (d)NDP, ribonucleoside and deoxyribonucleoside 5′-diphosphate; PP_i, pyrophosphate; P_i, orthophosphate.

Enzymatic Assays. Using (d)NDPs as substrates, DR_0079 produces the products (d)NMPs and orthophosphate (P_i). This enzymatic activity was determined by measuring the rate of release of P_i with the Malachite green reagent (*33*). The activity against (d)NDP substrates was measured in a reaction mixture (200 μL) containing 50 μM substrate, 50 mM Tris-HCl (pH 9.0), 7.5 mM $MgCl_2$, and 0.18 μM DR_0079 [1 μL from a stock solution in 50 mM Hepes and 100 mM NaCl (pH 7.0)]. As proposed previously for Nudix hydrolases (*34*), assays involving (d)NTPs included 10 microunits of inorganic pyrophosphatase to release P_i from any pyrophosphate (PP_i) produced by the enzyme. After the mixture had been incubated for 15 min at 37 °C, the reaction was terminated by addition of 50 μL of Malachite green reagent (*33*). The mixture was developed for 3 min at room temperature, and then absorption at 630 nm was measured with a Quant Universal Microplate Spectrophotometer (Bio-Tek Instruments, Inc.). The above reactions with CDP and CTP were performed in the presence and absence of inorganic pyrophosphatase to determine if PP_i or P_i was a product of the hydrolysis reaction. The optimum pH for the enzymatic reaction was determined using the method described above, CDP as the substrate, and three different buffers: Tris-HCl (pH 7.5−8.5), CHES-K (pH 8.6−10.0), and CAPS-K (pH 9.7−11.0). The optimal metal ion requirements for the hydrolysis of CDP were determined with the assay described above (pH 9), using 5 mM Mg^{2+} or another divalent cation (Mn^{2+}, Co^{2+}, Ni^{2+}, Zn^{2+}, Ca^{2+}, or Cu^{2+}) at 0.5 μM. Kinetic parameters were determined by nonlinear curve fitting using GraphPad Prism (version 4.00 for Windows; GraphPad Software, San Diego, CA).

Enzyme activity was also assayed using ^{31}P NMR spectroscopy by following the phosphorus resonances of three substrates, CDP, IDP, and CTP, and their products. Six hundred microliters of 5.0 mM CDP, CTP, and IDP (∼3000 nmol) was prepared in buffer containing 50 mM Tris and 10 mM $MgCl_2$ (pH 9.1). After a one-dimensional (1D) ^{31}P NMR spectrum was recorded on a Varian 600-Inova spectrometer at 37 °C, 9 μL of 1.2 mM DR_0079 (∼10 nmol, crystallization buffer) was added to the nucleotide diphosphate. Additional 1D ^{31}P spectra were then recorded immediately afterward (∼5 min delay) and at ∼10 min (NDP) or ∼60 min (NTP) intervals. To determine which phosphorus was undergoing substitution in the reaction, the experiments with CDP and CTP were repeated in the presence of 40% $H_2{}^{18}O$. The data were processed with Felix98 (MSI, San Diego, CA), and the ^{31}P chemical shifts were referenced to DSS (0 ppm) using indirect methods.

Crystallization. Crystals of SeMet-labeled DR_0079 were grown using vapor-diffusion, hanging drop, crystallization methods at room temperature (∼22 °C) using precipitants from Hampton Research (Aliso Viejo, CA). The best "coffin-like" crystals of SeMet-substituted DR_0079, identical in appearance to those reported for unlabeled DR_0079 (*31*), were harvested a couple days after 2 μL of protein (24 mg/mL) had been mixed with 2 μL of buffer containing 0.2 M calcium acetate hydrate, 0.1 M sodium cacodylate trihydrate, and 18% (w/v) polyethylene glycol 8000 (pH 6.5). To grow diffraction-quality crystals, it was critical that the protein concentration be >20 mg/mL.

Data Collection, Structure Determination, and Refinement. X-ray diffraction data for the DR_0079 crystals were collected at the National Synchrotron Light Source (NSLS), at Brookhaven National Laboratory, on beamline X29A using an ADSC Q315 CCD detector. A Se peak SAD data set at 2.04 Å resolution (SeMet-labeled) and a native data set at 1.9 Å resolution (unlabeled) were collected on orthorhombic crystals of DR_0079 (*31*). The images were integrated and scaled with HKL2000 (*35*). The heavy atom sites in the selenium-labeled DR_0079 were identified using the SHELX program suite (*36–38*) and HKL2MAP (*39*). The Se peak wavelength data set, which contained a useful anomalous signal out to 2.5 Å resolution, was used together with SOLVE (*40*) to produce an excellent electron density map at 2.5 Å resolution. Fragments of the structure were built automatically into the 2.5 Å resolution map using RESOLVE (*41*), and the remainder of the structure was built manually using XtalView/Xfit (*42*) and refined to 2.3 Å resolution. The model was further iteratively refined using a native data set extending out to 2.1 Å resolution and the refine.inp algorithm in CNS (*43*) employing the maximum likelihood target using amplitudes. Assessment of the quality of the stereochemistry of the final model, using PROCHECK (*44*) and MolProbity (*45*), indicated that the final model was a high-quality representation of the crystal structure of DR_0079 and represented an improvement over the NMR-derived structure. MolProbity analysis showed that the overall protein geometry of the final model ranked in the 84th percentile (MolProbity score of 1.77) with a clash score for "all-atom contacts" of 18.92. PROCHECK analysis of the crystal data showed that 94% of the φ and ψ pairs for DR_0079 were found in the most favored regions and 6% within additionally allowed regions, a marked improvement over the values of 65 and 29% observed for these regions, respectively, in the average NMR structure (*27*). The data collection and structure refinement statistics are given in Table 1, and the coordinates have been deposited in the Protein Data Bank (PDB) (entry 2O5F).

RESULTS AND DISCUSSION

Overall Structure of DR_0079. Two molecules of DR_0079 pack together in the asymmetric unit. The structure of each molecule in the asymmetric unit is similar with a backbone root-mean-square deviation (rmsd) of 0.81 Å and an all heavy atom rmsd of 1.23 Å as calculated using SuperPose (*46*). We will refer to only one subunit, B, when discussing the crystal structure of DR_0079 primarily because electron density was missing for residues S54−F60 in subunit A.

Figure 1A is a Molscript cartoon representation of the structure of DR_0079, and Figure 1B is a two-dimensional schematic of the secondary structure. The general secondary structure is similar to that observed in the NMR-based structure (*27*) aside from two short, three-residue, 3_{10}-helices (3_{10}-1 and 3_{10}-2) and an additional two-residue β-strand (β4*). The one additional β-strand has been labeled with an asterisk to facilitate comparison with the NMR-based structure. The molecule is composed of nine β-strands, three α-helices, and two 3_{10}-helices that can be grouped into three parts. β-Strands 1 and 2 along with 3_{10}-1 form an N-terminal β-sheet (residues 1−34); α-helices 3 and 4 form a C-terminal helix−turn−helix motif (residues 141−171), and the remainder of the molecule forms the Nudix core (residues 35−140). Within this Nudix core is the Nudix fold, a mixed

Table 1: Summary of Data Collection and Structure Refinement Statistics for DR_0079

	SeMet	native
space group	$C222_1$	$C222_1$
unit cell parameters	a = 35.46 Å, b = 157.62 Å, c = 127.03 Å $\alpha = \beta = \gamma = 90.0°$	a = 34.02 Å, b = 156.55 Å, c = 126.56 Å $\alpha = \beta = \gamma = 90.0°$
Matthews coefficient	2.3	2.2
percent solvent (%)	46.6	43.7
X-ray source	X29	X29
temperature (K)	100	100
resolution limits (Å)	50.0−2.04 (2.11−2.04)	50.0−1.90 (1.97−1.90)
detector distance (mm)	300	240
exposure time (s)	2	3
oscillation angle (deg)	0.5	0.5
no. of images	720	360
total angle (deg)	360	180
mosaicity (deg)	0.29−1.01	0.54−0.66
wavelength (Å)	0.9792	1.1000
no. of observations	226118 (4306)[a]	170690 (14245)[a]
no. of unique reflections	21753 (1305)[a]	27095 (2590)[a]
redundancy	10.4 (3.3)[a]	6.3 (5.5)[a]
completeness	91.4 (55.8)[a]	99.4 (97.8)[a]
$I/\sigma(I)$	24.8 (2.01)[a]	49.6 (8.5)[a]
R_{sym} (%)	10.6 (39.4)[a]	7.1 (26.8)[a]
	Structure Refinement	
PDB entry		2O5F
R_{conv} (%)		23.3
R_{free} (%)		26.7
no. of protein atoms		2538
no. of solvent atoms		171
no. of protein residues		316
average B value, protein atoms (Å^2)		29.1
average B value, main chain (Å^2)		26.7
average B value, solvent atoms (Å^2)		35.5
average B value, all atoms (Å^2)		29.5
root-mean-square deviation from ideal bond lengths (Å)		0.006
root-mean-square deviation from ideal bond angles (deg)		1.24
	Structure Validation	
PROCHECK		
Ramachandran		
favored		93.5
allowed		6.5
generous		0.0
disallowed		0.0
MolProbity		
clash score, all atoms (percentile)		18.9 (33rd)
clash score, atoms for which B < 40 (percentile)		17.1 (13th)
MER score (percentile)		1.8 (84th)

[a] Values in parentheses are for the highest-resolution shell.

β-sheet sandwiched between the catalytic helix (α1) and the orthogonally orientated N-terminal helix (α3). Such a general arrangement is observed in all Nudix proteins of known structure (*1, 21*). The mixed β-sheet of the Nudix fold is dominated by a "four"-strand mixed β-sheet with the central two β-strands parallel to each other. Such a general arrangement is also typical in all Nudix proteins of known structure. However, in DR_0079, one of the outer β-strands is discontinuous, composed of β5 and part of β4. In turn, β4 is the central β-strand in a small three-strand β-sheet with β4* and β8 that is attached to the outer edge of the four-strand mixed β-sheet.

A characteristic feature of all Nudix proteins is the highly conserved 23-residue Nudix box, $GX_5EX_7REUXEEXGU$, where U is a bulky hydrophobic group and X is any residue (*2, 3*). The Nudix sequence forms a loop−helix−loop motif (*47*) that is responsible for coordinating the catalytically essential divalent cation (usually Mg^{2+}) to the protein (*13, 14, 16, 20*). In DR_0079, the Nudix box is between G70 and V92, and as shown in Figure 2, it too adopts a loop−helix−loop structural motif. Of the 23 residues in the Nudix box, nine are highly conserved, $\underline{\mathbf{G}}^{70}X_5\underline{\mathbf{E}}^{76}X_7\underline{\mathbf{R}}^{84}\underline{\mathbf{E}}^{85}\underline{\mathbf{A}}^{86}X\underline{\mathbf{E}}^{88}\underline{\mathbf{E}}^{89}X\underline{\mathbf{N}}^{91}\underline{\mathbf{V}}^{92}$ (the superscript refers to the residue number in the DR_0079 Nudix sequence), and Figure 2 illustrates the relative orientation of these highly conserved residues in the loop−helix−loop Nudix motif. As observed in other Nudix structures, all the polar conserved residues in the α-helix are oriented on the same side and oppose the central mixed β-sheet. The side chains of A86 and V92 form a small hydrophobic pocket and likely play a conserved role in stabilizing the loop−helix−loop motif. The similar three-dimensional orientation of the conserved residues in all known Nudix protein structures suggests that these residues play similar roles in all Nudix hydrolases, binding one or more divalent cations (*48*). Indeed, it has been established that binding of the catalytic divalent metal ion occurs through the side chains of the glutamic acid residues in the loop−helix−loop Nudix motif (*13, 14, 16, 20, 49*). The enzyme-bound metal, in turn, forms a second sphere complex with the diphosphate part of the substrate as part of the

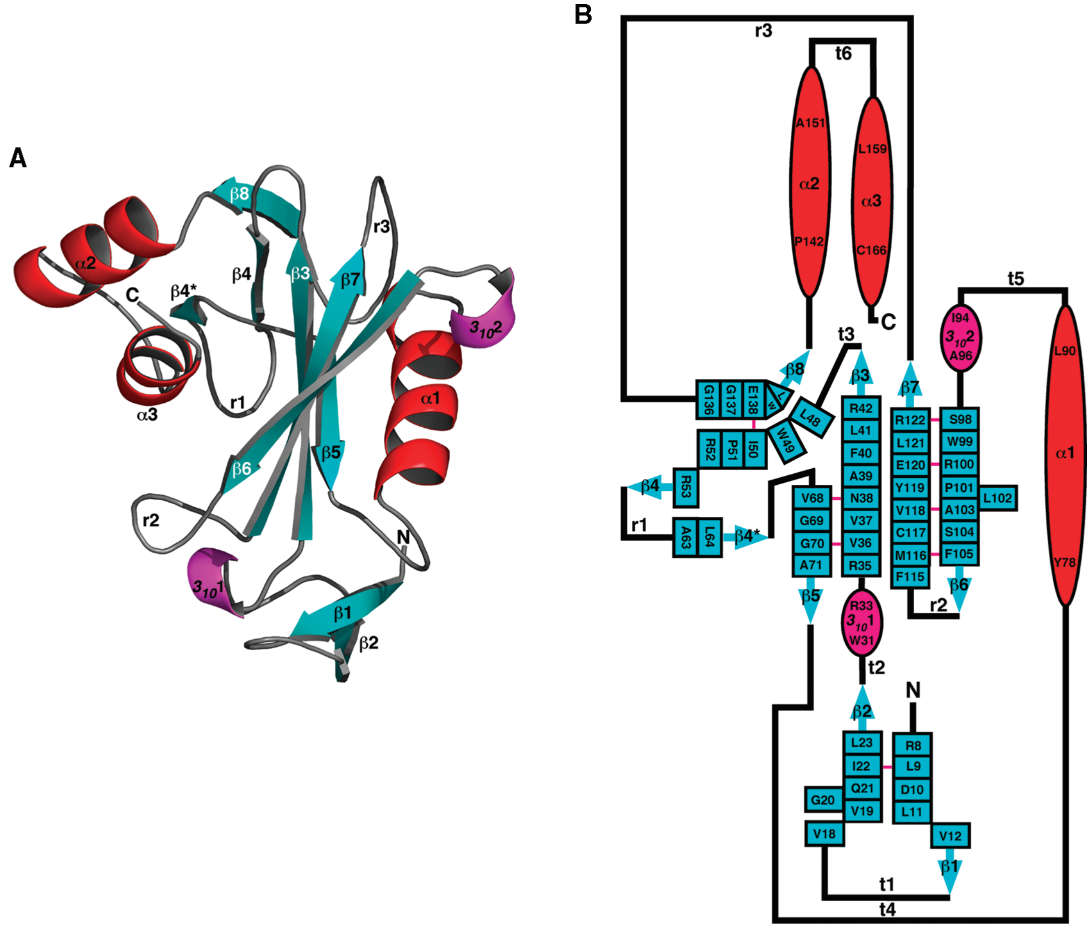

FIGURE 1: (A) Molscript ribbon representation of the crystal structure of DR_0079 in the metal-free form (PDB entry 2O5F). The β-strands are colored blue, α-helices red, and 3_{10}-helices magenta. Residues 1−34 make up the N-terminal antiparallel β-sheet, residues 35−140 the Nudix core, and residues 141−171 the C-terminal helix−turn−helix motif. (B) Secondary structure diagram of DR_0079. The α-helices are drawn as red ovals and 3_{10}-helices as magenta ovals with the residue number for the beginning and end of each element shown. The β-strands are drawn as solid blue arrows with each residue indicated within a box. The β-sheets contain bulges at residues G20 and L102. A solid pink line between β-sheet residues indicates dual hydrogen bonds between two residues in an antiparallel β-sheet.

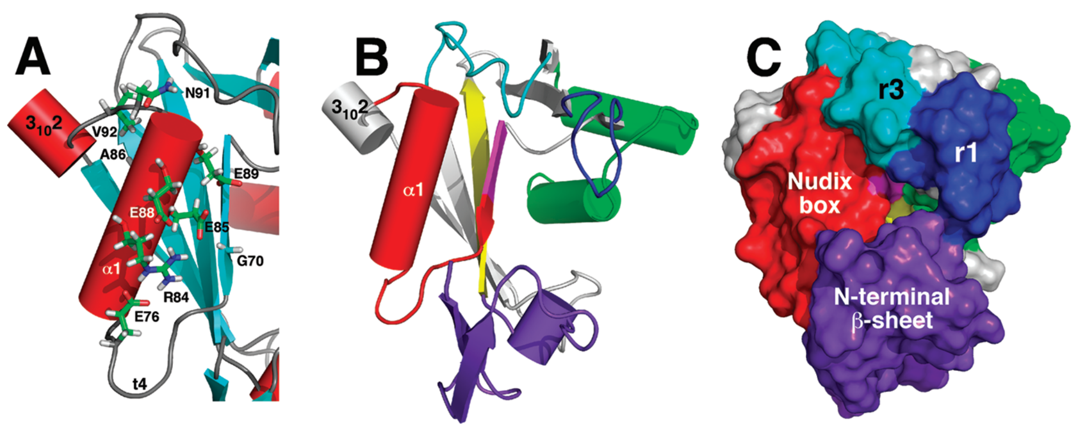

FIGURE 2: (A) Expansion of the loop−helix−loop Nudix box with the side chains of the nine highly conserved residues highlighted, labeled, and colored according to atom type. The regions that immediately surround the Nudix box are highlighted on the cartoon (B) and surface (C) structure of DR_0079. Red indicates the Nudix box, purple the N-terminal β-sheet, blue loop r1, cyan loop r3, magenta the rest of β5, yellow β3, and green the C-terminal helix−turn−helix loop.

enzyme's active site (*13*). While the diphosphate part of the Nudix substrate interacts with the loop−helix−loop Nudix motif and divalent metal cation, the other parts of the Nudix substrate, the nucleoside and a moiety x, interact with the side chains and motifs elsewhere in the protein (*13–16, 21, 50*). Differences in the shape and nature of the environment surrounding the Nudix box are responsible for the different substrate specificities of different Nudix hydrolases. As shown in Figure 2B, the immediate environment around the Nudix box is part of the N-terminal β-sheet, the backside of the mixed β-sheet, and loops r1 and r3. Note that no electron density was observed for residues S54−F60 in subunit A of the crystal structure, and amide cross-peaks were not observed for seven of the 14 possible resonances in the $^{1}H-^{15}N$ HSQC spectrum of this region, suggesting that the r1 region may be especially disordered in solution (*27, 51*).

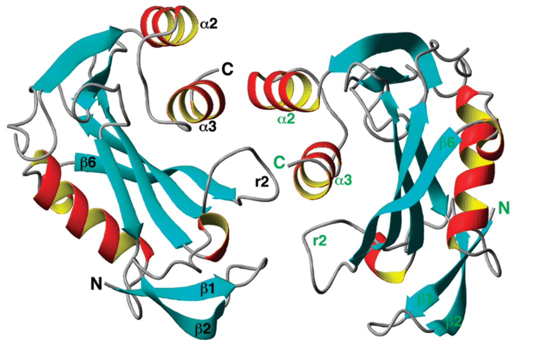

FIGURE 3: Molscript ribbon representation of two molecules of DR_0079 in the asymmetric unit highlighting the intermolecular interface. The β-strands are colored blue, the α- and 3_{10}-helices red, and the turns and loops gray.

Such intrinsically disordered regions are often sites of biological activity and become "ordered" only after binding their substrate (*52*).

Two molecules of DR_0079 pack together in the crystalline state as shown in Figure 3. Hydrophobic intermolecular contacts at three regions, between α3 and α2, r2 and α3, and t1 and r2, are responsible for holding the dimer together in the asymmetric unit. Dimeric Nudix hydrolases with extensive domain swapping have previously been observed, both in solution and in the crystalline state (*48*). For the proteins with extensive domain swapping, oligomerization is necessary for the biological function of the protein. However, the dimer observed in the DR_0079 crystal structure is likely a crystal packing artifact as NMR data and size exclusion chromatography strongly suggest that DR_0079 is a monomer in solution (*27, 28*). Furthermore, the buried surface area due to dimer formation in the asymmetric unit is small {[solvent accessible surface area (SASA) of individual monomers − SASA of the dimer in the asymmetric unit]/(SASA of individual monomers)} at <7%.

Enzymatic Studies of DR_0079. Purified DR_0079 was tested for enzymatic activity against a series of known Nudix hydrolase substrates (*34*), including (deoxy)nucleoside di- and triphosphates, nucleotide sugars and alcohols, and cofactors (FAD, NAD, and CoA) in the standard assay at a fixed substrate concentration of 5 mM. As illustrated in Figure 4A, CDP and CTP were the best substrates for DR_0079 followed by dCDP and dCTP. Note that while cytidine nucleotides were the favored substrate for DR_0079, the enzyme was still sufficiently promiscuous to show significant activity toward (d)GDP/GTP, (d)ADP/ATP, and (d)IDP/ITP [~20-fold difference between the poorest (IDP) and best (CDP) substrate]. There was no detectable activity against GDP-glucose/mannose, UDP-glucose/galactose, ADP-glucose, CDP-choline, CDP-ethanolamine, and CDP-glycerol (data not shown). Thus, DR_0079 is the first Nudix hydrolase selective for the cytidine nucleotides.

Like most known Nudix hydrolases (*1, 22*), DR_0079 had an alkaline pH optimum (pH 9.0−9.5) (data not shown) and required a divalent metal cation for activity. Figure 4B illustrates that Mg^{2+} was the most effective metal (optimal concentration of 7 mM), whereas Mn^{2+} and Co^{2+} supported lower activity (47 and 27%, respectively). Negligible activity was observed in the presence of Ni^{2+}, whereas Zn^{2+}, Ca^{2+}, and Cu^{2+} were inhibiting. Note that the result with Ca^{2+}

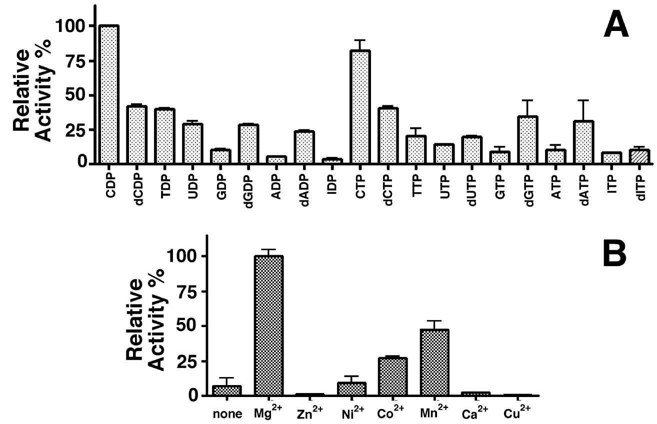

FIGURE 4: (A) Relative substrate activity of DR_0079 toward a variety of nucleoside di- and triphosphate substrates. (B) Nudix hydrolase activity of DR_0079 as a function of metal cation. The divalent cation requirements (metal profile) were determined toward CDP in the presence of 5 mM Mg^{2+} or another divalent cation (Mn^{2+}, Co^{2+}, Ni^{2+}, Zn^{2+}, Ca^{2+}, or Cu^{2+}) at 0.5 μM.

Table 2: Kinetic Parameters for DR_0079[a]

substrate	K_m (mM)	V_{max} [μmol min^{-1} (mg of protein)$^{-1}$]	k_{cat} (s^{-1})	k_{cat}/K_m (mM^{-1} s^{-1})
CDP	0.082 ± 0.011	5.18 ± 0.17	1.67	20.37
dCDP	0.092 ± 0.010	3.52 ± 0.11	1.12	12.17
TDP	0.105 ± 0.023	3.18 ± 0.27	1.03	9.81
UDP	0.137 ± 0.033	4.19 ± 0.42	1.35	9.85
GDP	0.092 ± 0.026	1.21 ± 0.10	0.39	4.24
dGDP	0.051 ± 0.010	1.55 ± 0.09	0.51	10.0
ADP	0.217 ± 0.033	0.93 ± 0.13	0.29	1.34
dADP	0.145 ± 0.028	1.61 ± 0.09	0.52	3.59
IDP	0.046 ± 0.010	0.21 ± 0.04	0.06	1.30
TTP	0.138 ± 0.030	2.13 ± 0.15	0.69	4.97
UTP	0.124 ± 0.030	1.65 ± 0.12	0.53	4.28
CTP	0.034 ± 0.007	1.82 ± 0.10	0.59	17.22
dCTP	0.023 ± 0.004	0.92 ± 0.08	0.30	12.83
ATP	0.317 ± 0.090	0.91 ± 0.08	0.29	0.92
dATP	0.062 ± 0.009	0.95 ± 0.07	0.31	4.92
GTP	0.394 ± 0.089	0.99 ± 0.13	0.32	0.81
dGTP	0.083 ± 0.011	1.25 ± 0.10	0.40	4.82
ITP	0.147 ± 0.027	0.55 ± 0.05	0.18	1.19
dITP	0.088 ± 0.008	0.68 ± 0.05	0.22	2.5

[a] All substrate concentrations were between 0.01 and 4.0 mM. Kinetic parameters were determined by nonlinear curve fitting using GraphPad Prism (version 4.00 for Windows).

corroborates the crystal structure that showed no metal was bound to DR_0079 despite the crystals being grown in the presence of 0.1 M $CaCl_2$. We also determined the kinetic parameters for the hydrolysis of various nucleotides by DR_0079. With all substrates, the protein exhibited classical Michaelis−Menten saturation kinetics with the lowest K_m with dCTP (K_m = 23.0 μM) and the highest activity with CDP (k_{cat} = 1.7 s^{-1}) (Table 2). Thus, DR_0079 demonstrated the highest catalytic efficiency toward CDP and CTP and is the first characterized Nudix hydrolase with such a substrate specificity.

The enzyme assays with (d)NDPs were first performed in the presence of inorganic pyrophosphatase to release P_i from any PP_i produced by DR_0079 because P_i is the component that reacts with the Malachite green reagent (*33*). To determine if DR_0079 was hydrolyzing (d)NDPs to nucleosides and PP_i or to (d)NMPs and P_i, the reaction with CDP was performed in the absence of inorganic pyrophosphatase and absorption at 630 nm measured. Absorption at 630 nm was still observed in the absence of inorganic pyrophosphatase, indicating that (d)NMPs and P_i were generated by DR_0079 upon hydrolysis of (d)NDPs [e.g., inorganic pyrophosphatase was not necessary for the enzyme assays with (d)NDPs]. On the other hand, when the enzyme assay with CTP was performed in the absence of inorganic pyrophosphatase, no absorption at 630 nm was observed, indicating that DR_0079 was converting (d)NTPs to (d)NMPs and PP_i.

To further verify the catalytic activity of DR_0079, to positively identify the hydrolysis products, and to determine the site of nucleophilic substitution by water, the reaction with CDP, IDP, and CTP was followed by ^{31}P NMR spectroscopy. The phosphorus chemical shifts of the nucleoside mono-, di-, and triphosphates are different, and hence, the reaction can be monitored in real time by following the changes in the ^{31}P NMR spectrum. The site of nucleophilic substitution can be determined by the small upfield shift (~0.02 ppm) in the phosphorus resonance upon formation of a single ^{31}P$-^{18}$O chemical bond (*12, 53*). An additional advantage of using ^{31}P NMR to follow hydrolysis by Nudix enzymes is that it eliminates the need for additional enzymes, such as inorganic pyrophosphatase, to release P_i.

As shown in Figure 5A, CDP contains two ^{31}P chemical shifts at -8.78 and -12.83 ppm that can be assigned to the β- and α-phosphorus atoms, respectively (*54, 55*). At the concentrations of DR_0079 used, the reaction was complete by the time the first 1D spectrum could be collected after its addition to the NMR tube as shown in Figure 5B. Two different resonances at 0.75 and 0.44 ppm were observed that correspond to CMP and P_i, respectively. To determine if the reaction was occurring via nucleophilic substitution of water on the α- or β-phosphorus, the reaction was repeated in the presence of $H_2{}^{18}O$-enriched (40%) water (*12*). As shown in the inset of Figure 5B, the orthophosphate (P_i) exhibited an additional upfield resonance ($\Delta = 0.02$ ppm) upon completion of the reaction. Such an observation establishes that the reaction occurs via a nucleophilic substitution at the β-phosphorus of CDP with CMP displaced as the leaving group (*12*). While CDP is a good substrate for DR_0079, Figure 4A showed that IDP is a relatively poor substrate, and this is evident in Figure 5D, the 1D ^{31}P NMR spectrum 50 min after the addition of DR_0079 to IDP in an NMR tube. Four resonances are observed corresponding to unhydrolyzed IDP (-8.83 and -12.88 ppm) and the hydrolysis products, IMP (0.77 ppm) and P_i (0.40 ppm).

As shown in Figure 5E, CTP contains three ^{31}P chemical shifts at -9.33, -14.14, and -25.04 ppm that can be assigned to the γ-, α-, and β-phosphorus atoms, respectively (*12, 54*). Figure 5F shows the spectrum 12 h after the addition of DR_0079 when the reaction is almost complete. Most of the α-, β-, and γ-phosphorus signals for GTP disappear completely while two new major resonances, corresponding to CMP (0.69 ppm) and PP_i (-10.02 ppm), appear. There is very little signal for P_i at 0.40 ppm. Indeed, this downfield region of the spectrum has been expanded in the inset of Figure 6F, and the intergrated intensity of both resonances indicates the amount of P_i relative to CMP is approximately 4%. Hence, the spectrum in Figure 5F unambiguously shows that very little CTP is converted to CMP by sequential hydrolysis of individual phosphorus atoms. Instead, the primary reaction is the hydrolysis of the ester bond between

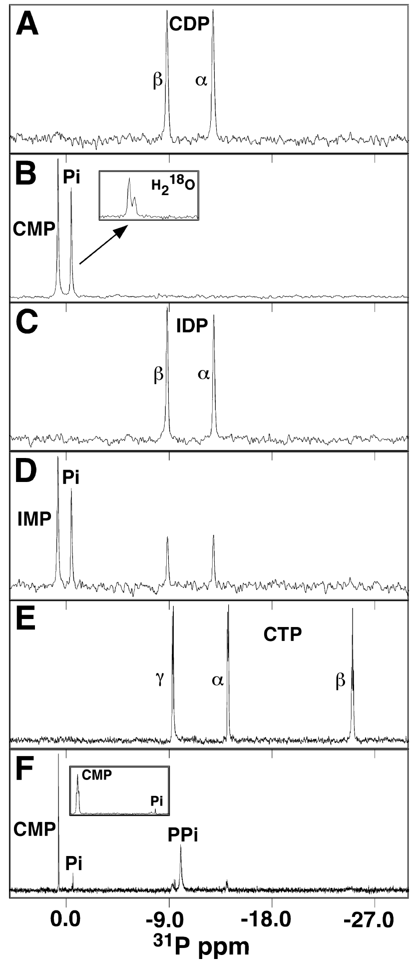

FIGURE 5: One-dimensional ^{31}P spectra of CDP, CTP, and IDP alone and at various times after the addition of DR_0079 to the NMR tube: (A) CDP alone, (B) CDP with DR_0079 immediately after protein addition with the inset showing an expansion (0.4 ppm) of the P_i resonance in the presence of 40% $H_2{}^{18}O$, (C) IDP alone, (D) CDP with DR_0079 after 50 min, (E) CTP alone, and (F) CTP with DR_0079 at the completion of the reaction (~12 h later) with the inset showing an expansion (0.5 ppm) of the downfield region. All spectra were recorded at a ^{1}H resonance frequency of 600 MHz at 37 °C in buffer containing 50 mM Tris and 10 mM $MgCl_2$ (pH 9.1).

the α- and β-phosphorus atoms of CTP. The repetition of this experiment in the presence of $H_2{}^{18}O$-enriched (40%) water resulted in a broadening of the PP_i resonance with no change in the CMP resonance (data not shown), indicating that the nucleophilic substitution of water was occurring on the β-phosphorus (*12*). Consequently, the hydrolysis of CTP by DR_0079 is likely occurring via a mechanism similar to the one reported for the hydrolysis of 8-oxo-dGTP by MutT (*12*), except the nucleotide binding pocket has a preference for cytosine di- and triphosphates over 7,8-dihydro-8-oxoguanosine triphosphate.

Co^{2+} Chemical Shift Mapping. Previous ^{1}H$-^{15}$N HSQC experiments with ^{15}N-labeled DR_0079 in the absence and presence of a 5-fold molar excess of EDTA suggested that DR_0079 was prepared in the metal-free form (*27*). This conclusion is corroborated by the biochemical data presented here showing that a divalent cation must be added to the protein before statistically significant activity is observed. This is also corroborated by the X-ray structure presented here showing no divalent cation bound to the protein

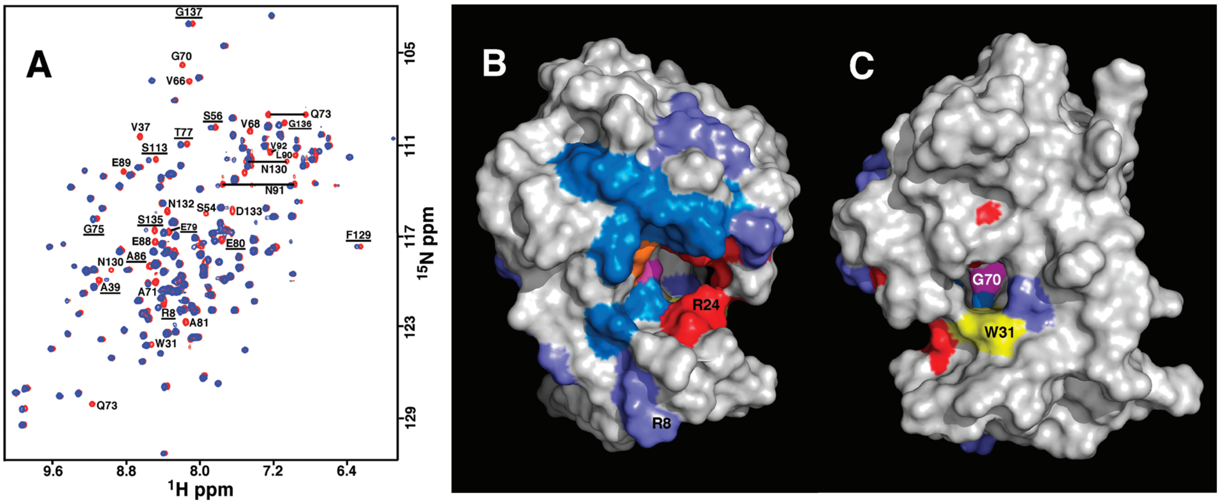

FIGURE 6: (A) Overlay of the ^{1}H−^{15}N HSQC spectra of DR_0079 in the absence (red) and presence (blue) of an ~1:1 molar ratio of $CoCl_2$. The chemical shifts of backbone amide and identified side chain amine resonances that disappear or shift (underlined) upon addition of $CoCl_2$ are labeled. Spectra were collected at a ^{1}H resonance frequency of 900 MHz at 25 °C in buffer containing 100 mM KCl, 20 mM potassium phosphate, and 2 mM DTT (pH 7.1). (B and C) Resonances for residues that disappear (marine blue) or move (slate) upon addition of $CoCl_2$ to DR_0079 are mapped onto the structure (2O5F) and shown in two orientations that differ by ~180°. The metal cation may rest over G70 (magenta), the residue with the largest chemical shift perturbation upon addition of $MgCl_2$ (*27*). Next to it, colored orange, is E85, the nearest glutamic acid side chain (the $^{1}H^{N}$ resonance of E85 overlaps with A160, and it is not possible to determine if this residue disappears upon addition of CoC_2). In the cleft there is a ring of lysine and arginine residues, and these are colored red (R24, R53, K57, and K156). Directly behind the ring of positively charged residues is an aromatic tryptophan side chain (W31) that is colored yellow in orientation A. This tryptophan's location in the cleft is more obvious in orientation B.

(although Mg^{2+} would be difficult to detect). Changes were previously observed in the ^{1}H−^{15}N HSQC spectrum of DR_0079 in the presence of a 100-fold molar excess of $MgCl_2$, while in the presence of a 25-fold molar excess of $MnCl_2$, DR_0079 precipitated out of solution (*27*). In light of the data shown in Figure 4B, and because excess $MgCl_2$ was necessary to observe significant chemical shift perturbations to the ^{1}H−^{15}N HSQC spectrum of DR_0079, the chemical shift perturbation experiments were repeated using $CoCl_2$ to better characterize the metal binding site on the protein. This technique is based on the premise that protein−ligand interactions perturb the chemical environment of the nuclei at the interface of ligand binding. Because such perturbations are often accompanied by changes in the chemical shifts of the backbone $^{1}H^{N}$ and ^{15}N resonances (*30, 56*), by identifying resonances that undergo a binding-dependent chemical shift or intensity perturbation, we are able to identify ligands that bind to a protein and to map the location of the ligand binding site on the three-dimensional structure of the protein. The ^{1}H−^{15}N HSQC spectrum of DR_0079 should be more sensitive to chemical shift perturbations upon binding Co^{2+} instead of Mg^{2+} because Co^{2+} is paramagnetic. Consequently, in addition to any chemical shift perturbations due to structural changes effected by divalent cation binding, the unpaired electrons in Co^{2+} can also affect the surrounding nuclear environment in two other major ways. One is a through-bond scalar interaction, known as a contact shift, which can propagate a maximum of five bonds from the metal center. The second is a through-space dipolar interaction, known as a pseudocontact shift, that propagates to neighboring nuclei with a $1/r^3$ distance dependence (*30, 57*). Figure 6A overlays the ^{1}H−^{15}N HSQC spectra of DR_0079 in the presence (blue) and absence (red) of 1 molar equiv of $CoCl_2$ and shows that a substantial subset of backbone, amide cross-peaks either disappear (16) or shift (12) in the presence of the divalent metal cation. In contrast, the average chemical shift perturbation of only nine residues was observed to shift more than 0.05 ppm with the addition of $MgCl_2$ to DR_0079 (*27*). Of these Mg^{2+}-perturbed chemical shifts, the most significantly affected residue was G70, with R8, E89, and D95 affected moderately. The small number of residues with chemical shift perturbations and the small magnitude of the perturbations suggested that the global structure of the protein was not significantly altered upon binding of Mg^{2+}, consistent with the minor structural changes reported for other Nudix proteins upon addition of a divalent cation (*16, 20*). Evidently, the larger number of perturbations observed upon binding of Co^{2+} primarily reflects through-bond and through-space interactions that propagate from the metal's center.

Panels B and C of Figure 6 map the positions of the $^{1}H^{N}$ residues affected by the addition of $CoCl_2$ onto the crystal structure of DR_0079. All the amide residues perturbed by the addition of Co^{2+} are clustered together on one face of the molecule at, or near, the loop−helix−loop Nudix motif. Divalent cations have been identified in many of the known Nudix structures with the side chain carboxyl group of one or more glutamic acid residues in the loop−helix−loop Nudix motif participating in the metal ligation (*13, 14, 16, 20*). It is likely that at least one of the glutamic acid residues in the Nudix box of DR_0079 is participating in metal ligation. These glutamic residues are most likely E85, the residue commonly observed in most crystal structures with a metal (*21, 49*), and possibly E89, the second most commonly observed residue complexed to a metal in crystal structures (*21, 49*) and the glutamic acid amide in the Nudix box with the second-most significant chemical shift perturbation in the presence of Mg^{2+} (E85 overlaps with A160; therefore, it is not possible to identify chemical shift perturbations for this residue). Note that the residue disturbed most by Mg^{2+} binding was G70, and it also disappears in the presence of Co^{2+}. Glycine 70 is the first highly conserved residue of the Nudix box, and in other Nudix proteins, including DR_0079,

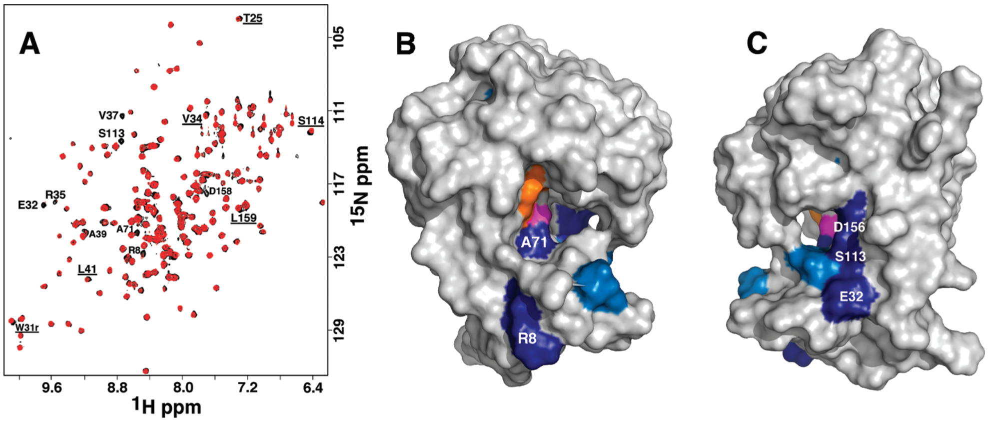

FIGURE 7: (A) Overlay of the ^{1}H$-^{15}$N HSQC spectra of DR_0079 in the absence (black) and presence (red) of an ~4:1 molar ratio of TMP-CP to DR_0079. The chemical shifts of backbone amide resonances that disappear or shift (underlined) upon addition of TMP-CP are labeled. Spectra were collected at a ^{1}H resonance frequency of 600 MHz at 25 °C in buffer containing 100 mM KCl, 100 mM $MgCl_2$, 20 mM potassium phosphate, and 2 mM DTT (pH 7.1). (B and C) Residues of backbone amides that disappear (dark blue) or shift slightly (light blue) upon addition of TMP-CP to DR_0079 at a substrate:protein molar ratio of ~4.0:1.0 are mapped unto the structure of DR_0079 and shown in two orientations that differ by ~180°. Also highlighted are E85 and E89 (orange), the residues that most likely bind the divalent cation, and G70 (magenta), the residue the cation may sit over.

this glycine residue is often preceded by a second glycine residue (*20, 34*). It has been suggested that these physically "small" glycine residues may be necessary to allow the metal to sit on the Nudix fold (*58*). The observation that the chemical shift for G70 is most perturbed in the presence of Mg^{2+} (*27*) and disappears completely in the presence of Co^{2+} supports the hypothesis that the metal may indeed be sitting over this residue in DR_0079.

Chemical Shift Mapping of the Substrate-Binding Surface with TMP-CP. Substrate screening indicated that (deoxy)-nucleoside diphosphates were the preferred substrate for DR_0079 with pyrimidine generally preferred over purine nucleotides. It is therefore not surprising that previous efforts to map the substrate-binding surface of DR_0079 using chemical shift perturbation methods with the nonhydrolyzable substrates AMPCPP and GMPPNP did not perturb the ^{1}H$-^{15}$N HSQC spectrum of DR_0079 since these substrates contained purines and they were triphosphates. It is also likely that the excess phosphate in the NMR buffer, at a 100-fold molar excess relative to the protein, did not affect the chemical shift mapping experiments significantly as enzymatic studies showed that a 50000-fold molar excess of phosphate did not inhibit catalysis (data not shown). Consequently, chemical shift mapping experiments were performed with TMP-CP (chosen over the CMP analogue because it is commercially available) in the same NMR buffer used in the initial studies. Relative to TDP, the oxygen bridging the two phosphorus atoms is replaced with a methylene group in TMP-CP, and this prevents hydrolysis of the phosphodiester bond. Figure 7A shows the chemical shift perturbations of the ^{1}H$-^{15}$N HSQC spectrum of DR_0079 (black) upon addition of a 4-fold molar excess of TMP-CP (red) to the protein. The amide resonances for eight residues disappear completely, or their intensity is significantly reduced; there are slight perturbations to six additional residues. Note that at intermediate molar ratios there were no "perturbed only" cross-peaks, but there was a gradual decrease in intensity for the eight "disappearing" cross-peaks with an increase in TMP-CP concentration.

The data in Figure 7A are mapped onto the surface of DR_0079 in panels B and C of Figure 7. The positions of the ^{1}H^N residues that disappear, or where intensity decreases, at a 4:1 molar ratio of TMP-CP to DR_0079 are colored dark blue, while the positions of ^{1}H^N residues that are perturbed are colored light blue. As a reference, the likely primary metal binding glutamic acid residues, E85 and E89, are colored orange and the residue the metal likely sits over, G70, is colored magenta. In general, the residues perturbed by TMP-CP binding are near the metal binding site and the cleft adjacent to this site. Indeed, A71 is right next to the metal binding site. Three residues that disappear, E32, S113 and, D156, form a contiguous surface on the far side of the cleft as shown in Figure 7B. Residues in regions that immediately surround the metal binding core, r3, r1, and the N-terminal β-sheet, as illustrated in panels B and C of Figure 2, are not significantly perturbed following the addition of TMP-CP. As illustrated in Figure 4A, TDP is not the optimal substrate for DR_0079, and perhaps the binding is not very tight. Alternatively, pyrimidine nucleoside diphosphates are not very large molecules, and it may be that the binding of (d)NDPs to DR_0079 does not affect significant perturbations to the protein.

Speculative Substrate Binding Events. Using the available chemical shift data, the crystal structure for DR_0079, and the knowledge of how other Nudix substrates bind to proteins, it is possible to speculate about which regions and residues in DR_0079 might play a role in binding (d)NDPs. Foremost, DR_0079 has a well-defined pocket at the mouth of the Nudix box, illustrated best in Figure 6B. Differences in the features of such pockets are responsible for the substrate specificity of different Nudix proteins (*21, 27*). Next, the Co^{2+} chemical shift mapping data presented here and the data previously reported for Mg^{2+} (*27*) suggest that at least one divalent metal cation sits over G70 and it could be held in position by the side chains of E85 and/or E95. As observed in other Nudix protein$-$substrate complexes, this metal probably coordinates with the phosphodiester group of the substrate, either directly or via a second sphere of water (*13*). Surrounding the hydrophobic part of the substrate binding cleft in Nudix proteins of known structure are polar residues that form hydrogen bonds with the nucleoside and/or interact with the sugar and phosphate groups of the substrate (*21*). While four polar residues, R24, R53, K57, and K156, surround the metal binding site (Figure 6B), no perturbations of these residues were observed upon binding to TMP-CP (Figures 7), and therefore, there is no evidence that they participate in the catalysis. The substrate binding cleft in Nudix proteins of known structure also often contains a hydrophobic surface that interacts with the hydrophobic parts of the substrate, especially with regard to "base stacking"-like interactions with the nucleoside base (*16, 27*). The side chain of W31 sits on the "floor" of the substrate binding cleft (Figure 6B) next to the ring of polar residues in DR_0079. While no chemical shift perturbations were directly observed for the backbone amide of W31 upon addition of TMP-CP, the intensities of backbone amides of residues around this region (E32, S113, and D156) were affected (Figure 7B), suggesting that some type of interaction with the substrate may be occurring on this face of the protein.

Biological Function. While the substrates tested here show that DR_0079 has a marked preference for (d)CDP and (d)CTP nucleotides, such in vitro testing for biological function is limited to the number of potential substrates available for study (*22*). For example, DR_0079 may have yet greater specificity for an untested, oxidized (d)CDP or (d)CTP. This problem is compounded because Nudix hydrolases generally exhibit overlapping substrate specificity (*1, 34*). Indeed, such overlapping specificity will make it difficult to test biological functionality in vivo by systematic gene disruption in *D. radiodurans* because when a specific Nudix hydrolase is knocked out another one (or more) of the 20 Nudix hydrolases may substitute (*22*).

The structure of DR_0079 represents the first Nudix hydrolyase to show a preference for cytidine (deoxy)nucleoside 5′-diphosphates. To identify other proteins with similar substrate specificities, the Protein Data Bank was searched with Dali (*59*) for structures with similarities to DR_0079. Thirty-one proteins with Z scores of >4 were identified. All of the proteins, except two, are suspected Nudix hydrolases or known Nudix hydrolases with substrate specificities that vary across the known Nudix substrate range. The structure with the highest Z score, 19.8, is the crystal structure of the putative Nudix hydrolase yfcD from *E. coli* strain K12 (PDB entry 2FKB). The function of this protein is unknown (*25*), but it contains an N-terminal β-sheet and C-terminal helix−turn−helix motif (in this case it is a helix−helix−helix motif) that is very similar to DR_0079. Perhaps the similarities in the structure of DR_0079 and yfcD will reflect a similar preference for nucleoside diphosphates. On the other hand, it may not, as the next two highest Z scores, 18.1 and 17.1, were for type I isopentenyl-diphosphate δ-isomerase (IDI) from *E. coli* (*60*). This enzyme is an important component of the ubiquitous sterol/isoprenoid biosynthetic pathway, catalyzing the interconversion of isopentenyl diphosphate and dimethylallyl diphosphate. However, these compounds were ruled out as substrates for DR_0079 for a number of compelling reasons, most important of which was a negative result when testing for IPP isomerase activity (*27*). Consequently, the large number of DALI "hits" with DR_0079 may simply reflect similarities in the basic Nudix fold that concomitantly may result in overlap of substrate specificities.

Comparison to the Structures of Other D. radiodurans Nudix Proteins. The genome of the bacterium *D. radiodurans* encodes 21 Nudix hydrolases containing a fully conserved Nudix box (*61*). Crystal structures have been determined for three of these gene products: DR1184 (*20*), DR1025 (*49*), and now DR_0079. There is convincing evidence that the native substrate for DR1184 is coenzyme A (*20*), the native substrate for DR1025 is uncertain but it has been cocrystallized with both a GTP analogue and Ap_4A (*49*), and DR_0079 shows a perference for (d)CDP and (d)CTP. Given different preferred substrates for each *D. radiodurans* hydrolase, it is not surprising that while the same basic Nudix fold, the mixed four-strand β-sheet sandwiched between orthogonal α-helices, is similar in all three proteins, the length and nature of the folds and appendages connected to the four-strand β-sheet differ. In DR_1184, the appendages are an N-terminal α-helix followed by a β-strand, an extra three-strand β-sheet attached to the four-strand β-sheet, and an α-helix and three-strand antiparallel β-sheet inserted near the C-terminus. In DR_1025, these appendages are a short N-terminal helix, a small three-strand β-sheet attached to the four-strand β-sheet, and an extra α-helix near the C-terminus. In DR_0079, these appendages are an N-terminal antiparallel β-sheet (β1 and β2), an extra three-strand β-sheet (β4, β4*, and β8) attached to the four-strand β-sheet, and an α-helix (α2) inserted near the C-terminus. The structural and functional diversity of these three proteins, despite their sequence similarities, highlights the need to explore the diversity in protein families with the same basic fold but differing sequence and function (*49*).

The Nudix hydrolase DR_0975 has a marked specificity for (d)NDPs and is nearly the same length as DR_0079 at 169 versus 171 residues. Could the overall structure of both proteins be similar, especially with regard to the substrate binding site? While some details of the substrate binding cleft may be similar between the proteins, the overall structure will likely differ because the first residue of the Nudix box in DR_0079 is G70 while the first residue in DR_0975 is G40. Consequently, the region N-terminal to the Nudix box will be 30 residues shorter in DR_0975, while the region C-terminal to the Nudix box will be ∼30 residues longer.

Concluding Remarks. There had been great interest in the bacterium *D. radiodurans* because of its unique capacity to withstand relatively high doses of ionizing radiation and the lethal and mutagenic effects of ultraviolet radiation and other physical and chemical DNA-damaging agents (*62, 63*). Such properties likely are a consequence of the organism's ability to tolerate desiccation (*64*). Another unique property of *D. radiodurans* is that its genome contains an uncommonly large number of genes with potential DNA repair activities (*61*). Consequently, it has been suggested that *D. radiodurans* desiccation−radiation tolerance is related to the redundancy in DNA repair genes that include the 21 genes with sequence homology to the Nudix family of polyphosphate pyrophosphohydrolases (*3*). However, emerging evidence suggests that DNA repair is not the primary function of the Nudix hydrolase suite of proteins in *D. radiodurans*. A transcriptomic study indicated that only five of the 21 *D. radiodurans* genes were induced following exposure to γ-irradiation (*65*). Global analysis of the *D. radiodurans* proteome using high-resolution mass spectrometry methods showed that DR_0079 and the 20 other hypothetical Nudix proteins were predominately expressed in unstressed cells (*66*). Induction assays showed that neither peroxide nor superoxide induced the expression of the Nudix hydrolase DR_0975 in *D. radiodurans* (*22*). Instead of the repair of oxidized DNA, the primary function of the Nudix hydrolases may be to maintain the physiological balance in the cell during the hours of chromosomal repair immediately following exposure to ionizing radiation or stress by removing or inactivating potentially toxic endogenous metabolites that contain at least one diphosphate linkage (*9, 34*). The promiscuous nature of many of these hydrolases, especially toward oxidized nucleosides, may enhance their housekeeping role. With regard to "keeping house", it has been observed that *D. radiodurans* cells in stationary phase are more resistant to radiation than cells in logarithmic phase (*67*). Because induction assays show that DR_0975 expression is induced only upon entry of cells into the stationary phase, the housekeeping duties that DR_0975 performs to prepare the cell for the stationary phase may indirectly contribute to the organism's radiation resistant properties (*22*). Further biochemical studies are necessary to determine if the specificity of DR_0079 for cytosine ribonucleoside 5′-diphosphate (CDP) and cytosine ribonucleoside 5′-triphosphate (CTP) is part of its in vivo housekeeping duties.

ACKNOWLEDGMENT

We thank Dr. Stephen R. Holbrook at Lawrence Berkeley National Laboratory (Berkeley, CA) for first getting us involved in studies on *D. radiodurans* Nudix hydrolases and Dr. Richard D. Smith's group at Pacific Northwest National Laboratory for providing us with $H_2{}^{18}O$.

REFERENCES

1. McLennan, A. G. (2006) The Nudix hydrolase superfamily. *Cell. Mol. Life Sci. 63*, 123–143.
2. Abeygunawardana, C., Weber, D. J., Gittis, A. G., Frick, D. N., Lin, J., Miller, A. F., Bessman, M. J., and Mildvan, A. S. (1995) Solution structure of the MutT enzyme, a nucleoside triphosphate pyrophosphohydrolase. *Biochemistry 34*, 14997–15005.
3. Bessman, M. J., Frick, N., and O'Handley, S. F. (1996) The MutT proteins or "Nudix" hydrolases, a family of versatile, widely distributed, "housecleaning" enzymes. *J. Biol. Chem. 271*, 25059–25062.
4. Wang, Z., Jiao, X., Carr-Schmid, A., and Kiledjian, M. (2002) The hDcp2 protein is a mammalian mRNA decapping enzyme. *Proc. Natl. Acad. Sci. U.S.A. 99*, 12663–12668.
5. Dunn, C. A., O'Handley, S. F., Frick, D. N., and Bessman, M. J. (1999) Studies on the ADP-ribose pyrophosphatase subfamily of the nudix hydrolases and tentative identification of trgB, a gene associated with tellurite resistance. *J. Biol. Chem. 274*, 32318–32324.
6. Lawhorn, B. G., Gerdes, S. Y., and Begley, T. P. (2004) A genetic screen for the identification of thiamin metabolic genes. *J. Biol. Chem. 279*, 43555–43559.
7. Safrany, S. T., Caffrey, J. J., Yang, X. N., Bembenek, M. E., Moyer, M. B., Burkhart, W. A., and Shears, S. B. (1998) A novel context for the 'MutT' module, a guardian of cell integrity, in a diphosphoinositol polyphosphate phosphohydrolase. *EMBO J. 17*, 6599–6607.
8. Xu, W., Jones, C. R., Dunn, C. A., and Bessman, M. J. (2004) Gene ytkD of *Bacillus subtilis* encodes an atypical nucleoside triphosphate member of the Nudix hydrolase superfamily. *J. Bacteriol. 186*, 8380–8384.
9. Galperin, M. Y., Moroz, O. V., Wilson, K. S., and Murzin, A. G. (2006) House cleaning, a part of good housekeeping. *Mol. Microbiol. 59*, 5–19.
10. Grollman, A. P., and Moriya, M. (1993) Mutagenesis by 8-oxoguanine: An enemy within. *Trends Genet. 9*, 246–249.
11. Maki, H., and Sekiguchi, M. (1992) MutT protein specifically hydrolyzes a potent mutagenic substrate for DNA synthesis. *Nature 355*, 273–275.
12. Weber, D. J., Bhatnagar, S. K., Bullions, L. C., Bessman, M. J., and Mildvan, A. S. (1992) NMR and isotopic exchange studies of the site of bond cleavage in the MutT reaction. *J. Biol. Chem. 267*, 16939–16942.
13. Lin, J., Abeygunawardana, C., Frick, D. N., Bessman, M. J., and Mildvan, A. S. (1997) Solution structure of the quaternary MutT-M^{2+}-AMPCPP-M^{2+} complex and mechanism of its pyrophosphohydrolase action. *Biochemistry 36*, 1199–1211.
14. Bailey, S., Sedelnikova, S. E., Blackburn, G. M., Abdelghany, H. M., Baker, P. J., McLennan, A. G., and Rafferty, J. B. (2002) The crystal structure of diadenosine tetraphosphate hydrolase from *Caenorhabditis elegans* in free and binary complex forms. *Structure 10*, 589–600.
15. Fletcher, J. I., Swarbrick, J. D., Maksel, D., Gayler, K. R., and Gooley, P. R. (2002) The structure of Ap(4)A hydrolase complexed with ATP-MgF(x) reveals the basis of substrate binding. *Structure 10*, 205–213.
16. Gabelli, S. B., Bianchet, M. A., Bessman, M. J., and Amzel, L. M. (2001) The structure of ADP-ribose pyrophosphatase reveals the structural basis for the versatility of the Nudix family. *Nat. Struct. Biol. 8*, 467–472.
17. Kang, L.-W., Gabelli, S. B., Cunningham, J. E., O'Handley, S. F., and Amzel, L. M. (2003) Structure and mechanism of MT-ADPRase, a Nudix hydrolase from *Mycobacterium tuberculosis*. *Structure 11*, 1015–1023.
18. Zha, M., Zhong, C., Peng, Y., Hu, H., and Ding, J. (2006) Crystal structure of human NUDT5 reveals insights into the structural basis of the substrate specificity. *J. Mol. Biol. 364*, 1021–1033.
19. Gabelli, S. B., Bianchet, M. A., Xu, W., Dunn, C. A., Niu, Z. D., Amzel, L. M., and Bessman, M. J. (2007) Structure and function of the *Escherichia coli* dihydroneopterin triphosphate pyrophosphatase: A Nudix enzyme involved in folate biosynthesis. *Structure 15*, 1014–1022.
20. Kang, L.-W., Gabelli, S. B., Bianchet, M. A., Xu, W. L., Bessman, M. J., and Amzel, L. M. (2003) Structure of a coenzyme A pyrophosphatase from *Deinococcus radiodurans*: A member of the Nudix family. *J. Bacteriol. 185*, 4110–4118.
21. Mildvan, A. S., Xia, Z., Azurmendi, H. F., Saraswat, V., Legler, P. M., Massiah, M. A., Gabelli, S. B., Bianchet, M. A., Kang, L.-W., and Amzel, L. M. (2005) Structures and mechanisms of Nudix hydrolases. *Arch. Biochem. Biophys. 433*, 129–143.
22. Fisher, D. J., Cartwright, J. L., Harashima, H., Kamiya, H., and McLennan, A. G. (2004) Characterization of a Nudix hydrolase from *Deinococcus radiodurans* with a marked specificity for deoxyribonucleoside 5′-diphosphates. *BMC Biochem. 5*, 7–14.
23. Ishibashi, T., Hayakawa, H., and Sekiguchi, M. (2003) A novel mechanism for preventing mutations caused by oxidation of guanine nucleotides. *EMBO Rep. 4*, 479–483.
24. Hori, M., Fujikawa, K., Kasai, H., Harashima, H., and Kamiya, H. (2005) Dual hydrolysis of diphosphate and triphosphate derivatives of oxidized deoxyadenosine by Orf17 (NtpA), a MutT-type enzyme. *DNA Repair 4*, 33–39.
25. Xu, W., Dunn, C. A., O'Handley, S. F., Smith, D. L., and Bessman, M. J. (2006) Three new Nudix hydrolases from *Escherichia coli*. *J. Biol. Chem. 281*, 22794–22798.
26. Ito, R., Hayakawa, H., Sekiguchi, M., and Ishibashi, T. (2005) Multiple enzyme activities of *Escherichia coli* MutT protein for sanitization of DNA and RNA precursor pools. *Biochemistry 44*, 6670–6674.
27. Buchko, G. W., Ni, S., Holbrook, S. R., and Kennedy, M. A. (2004) Solution structure of hypothetical Nudix hydrolase DR0079 from extremely radiation-resistant *Deinococcus radiodurans* bacterium. *Proteins 56*, 28–39.
28. Buchko, G. W., Ni, S., Holbrook, S. R., and Kennedy, M. A. (2003) ^{1}H, ^{13}C, and ^{15}N NMR assignments of the hypothetical Nudix protein DR0079 from the extremely radiation-resistant bacterium *Deinococcus radiodurans*. *J. Biomol. NMR 25*, 169–170.
29. Zuiderweg, E. R. P. (2002) Mapping protein-protein interactions in solution by NMR spectroscopy. *Biochemistry 41*, 1–7.
30. Buchko, G. W., Daughdrill, G. W., de Lorimier, R., Rao, B. K., Isern, N. G., Lingbeck, J. M., Taylor, J. S., Wold, M. S., Gochin, M., Spicer, L. D., Lowry, D. F., and Kennedy, M. A. (1999) Interactions of human nucleotide excision repair protein XPA with

DNA and RPA70ΔC327: Chemical shift mapping and ^{15}N NMR relaxation studies. *Biochemistry 38*, 15116–15128.

31. Holbrook, E. L., Schulze-Gahmen, U., Buchko, G. W., Ni, S., Kennedy, M. A., and Holbrook, S. R. (2003) Purification, crystallization and preliminary X-ray analysis of two Nudix hydrolases from *Deinococcus radiodurans*. *Acta Crystallogr. D59*, 737–740.
32. Doublie, S. (1997) Preparation of selenomethionyl proteins for phase determination. *Methods Enzymol. 276*, 523–530.
33. Baykov, A. A., Evtushenko, O. A., and Avaeva, S. M. (1988) A malachite green procedure for orthophosphate determination and its use in alkaline phosphatase-based enzyme immunoassay. *Anal. Biochem. 171*, 266–270.
34. Xu, W., Shen, J., Dunn, C. A., Desai, S., and Bessman, M. J. (2001) The Nudix hydrolases of *Deinococcus radiodurans*. *Mol. Microbiol. 39*, 286–290.
35. Otwinowski, Z., and Minor, W. (1997) Processing of X-ray diffraction data collected in oscillation mode. *Methods Enzymol. 276*, 307–326.
36. Schneider, T. R., and Sheldrick, G. M. (2002) Substructure solution with SHELXD. *Acta Crystallogr. D58*, 1772–1779.
37. Sheldrick, G. M. (2002) Macromolecular phasing with SHELXE. *Z. Kristallogr. 217*, 644–650.
38. Sheldrick, G. M. (2003) SHELXC.
39. Pape, T., and Schneider, T. R. (2004) HKL2MAP: A graphical user interface for phasing with SHELX programs. *J. Appl. Crystallogr. 37*, 843–844.
40. Terwilliger, T. C., and Berendzen, J. (1999) Automated MAD and MIR structure solution. *Acta Crystallogr. D55*, 849–861.
41. Terwilliger, T. C. (2001) Map-likelihood phasing. *Acta Crystallogr. D57*, 1763–1775.
42. McRee, D. E. (1999) A versatile program for manipulating atomic coordinates and electron density. *J. Struct. Biol. 125*, 156–165.
43. Brünger, A. T., Adams, P. D., Clore, G. M., Delano, W. L., Gros, P., Grosse-Kunstleve, R. W., Jiang, J.-S., Kuszewski, J., Nilges, M., Pannu, N. S., Read, R. J., Rice, L. M., Simonson, T., and Warren, G. (1998) Crystallography and NMR System (CNS): A new software suite for macromolecular structure determination. *Acta Crystallogr. D54*, 905–921.
44. Laskowski, R. A., MacArthur, M. W., Moss, D. S., and Thornton, J. M. (1993) PROCHECK: A program to check the sterochemical quality of protein structures. *J. Appl. Crystallogr. 26*, 283–291.
45. Lovell, S. C., Davis, I. W., Arendall, W. B., III, de Bakker, P. I. W., Word, J. M., Prisant, M. G., Richardson, J. S., and Richardson, D. L. (2003) Structure validation by C-α geometry: φ, ψ, and C-β deviation. *Proteins 50*, 437–450.
46. Maiti, R., van Domselaar, G. H., Zhang, H., and Wishart, D. S. (2004) SuperPose: A simple server for sophisticated structural superposition. *Nucleic Acids Res. 32*, W590–W594.
47. Koonin, E. V. (1993) A highly conserved sequence motif defining the family of MutT-related proteins from eubacteria, eukaryotes and viruses. *Nucleic Acids Res. 21*, 4847.
48. Wang, S., Mura, C., Sawaya, M. R., Cascio, D., and Eisenberg, D. (2002) Structure of a Nudix protein from *Pyrobaculum aerophilum* reveals a dimer with two intersubunit β-sheets. *Acta Crystallogr. D58*, 571–578.
49. Ranatunga, W., Hill, E. E., Mooster, J. L., Holbrook, E. L., Schulze-Gahmen, U., Xu, W., Bessman, M. J., Brenner, S. E., and Holbrook, S. R. (2004) Structural studies of the Nudix hydrolase DR1025 from *Deinococcus radiodurans* and its ligand complexes. *J. Mol. Biol. 339*, 103–116.
50. Massiah, M. A., Saraswat, V., Azurmendi, H. F., and Mildvan, A. S. (2003) Solution structure and NH exchange studies of the MutT pyrophosphohydrolase complexed with Mg^{2+} and 8-oxo-dGMP, a tightly bound product. *Biochemistry 42*, 10140–10154.
51. Stogios, P. J., Chen, L., and Prive, G. G. (2007) Crystal structure of the BTB domain from the LRF/ZBTB7 transcriptional regulator. *Protein Sci. 16*, 336–342.
52. Dunker, A. K., Brown, C. J., Lawsor, J. D., Iahoucheva, L. M., and Obradovic, Z. (2002) Intrinsic disorder and protein function. *Biochemistry 41*, 6573–6582.
53. Cohn, M., and Hu, A. (1978) Isotopic (^{18}O) shift in ^{31}P nuclear magentic resonance appied to a study of enzyme-catalyzed phosphate-phosphate exchange and phosphate (oxygen)-water exchange reactions. *Proc. Natl. Acad. Sci. U.S.A. 75*, 200–203.
54. Cohn, M., and Hughes, T. R. (1960) Phosphorus magnetic resonance spectra of adenosine di- and triphosphate. *J. Biol. Chem. 235*, 3250–3253.
55. Tran-Dinh, S., and Neumann, J. M. (1977) A ^{31}P-NMR study of the interaction of Mg^{2+} with nucleoside diphosphates. *Nucleic Acids Res. 4*, 397–403.
56. Shukar, S. B., Hajduk, P. J., Meadows, R. P., and Fesik, S. W. (1996) Discovering high-affinity ligands for proteins. *Science 274*, 1531–1534.
57. Gochin, M., and Roder, H. (1995) Protein structure refinement based on paramagnetic NMR shifts: Applications to wild-type and mutant forms of cytochrome c. *Protein Sci. 4*, 296–305.
58. Lin, J., Abeygunawardana, C., Frick, D. N., Bessman, M. J., and Mildvan, A. S. (1996) The role of Glu 57 in the mechanism of the *Escherichia coli* MutT enzyme by mutagenesis and heteronuclear NMR. *Biochemistry 35*, 6715–6726.
59. Holm, L., and Sander, C. (1998) Touring protein fold space with Dali/FSSP. *Nucleic Acids Res. 26*, 316–319.
60. Bonanno, J. B., Edo, C., Eswar, N., Pieper, U., Romanowski, M. J., Ilyin, V., Gerchman, S. E., Kycia, H., Studier, F. W., Sali, A., and Burley, S. K. (2001) Structural genomics of enzymes involved in sterol/isoprenoid biosynthesis. *Proc. Natl. Acad. Sci. U.S.A. 98*, 12896–12901.
61. White, O., Eisen, J. A., Heidelberg, J. F., Hickey, E. K., Peterson, J. D., Dodson, R. J., Haft, D. H., Gwinn, M. L., Nelson, W. C., Richardson, D. L., Moffat, K. S., Qin, H., Jiang, L., Pamphile, W., Crosby, M., Shen, M., Vamathevan, J. J., Lam, P., McDonald, L., Utterback, T., Zalewski, C., Makarova, K. S., Aravind, L., Daly, M. J., Minton, K. W., Fleischmann, R. D., Ketchum, K. A., Nelson, K. E., Salzberg, S., Smith, H. O., Venter, J. C., and Fraser, C. M. (1999) Genome sequence of the radioresistant bacterium *Deinococcus radiodurans* R1. *Science 286*, 1571–1577.
62. Anderson, A. W., Nordon, H. C., Cain, R. F., Parrish, G., and Duggan, D. (1956) Studies on a radio-resistant micrococcus. I. Isolation, morphology, cultural characteristics, and resistance to γ radiation. *Food Technol. 10*, 575–578.
63. Battista, A. (1997) Against all odd: The survival strategies of *Deinococcus radiodurans*. *Annu. Rev. Microbiol. 51*, 203–224.
64. Mattimore, V., and Battista, J. R. (1996) Radioresistance of *Deinococcus radiodurans*: Functions necessary to survive ionizing radiation are also necessary to survive prolonged desiccation. *J. Bacteriol. 178*, 633–637.
65. Liu, Y., Zhou, J., Omelchenko, M. V., Beliaev, A. S., Venkateswaran, A., Stair, J., Wu, L., Thompson, D. K., Xu, D., Rogozin, I. B., Gaidamakova, E. K., Zhai, M., Makarova, K. S., Koonin, E. V., and Daly, M. J. (2003) Transcriptome dynamics of *Deinococcus radiodurans* recovering from ionizing radiation. *Proc. Natl. Acad. Sci. U.S.A. 100*, 4193–4196.
66. Lipton, M. S., Pasa-Tolic, L., Anderson, G. A., Anderson, D. J., Auberry, D. L., Battista, J. R., Daly, M. J., Fredrickson, J., Hixson, K. K., Kostandarithes, H., Masselon, C., Markillie, L. M., Moore, R. J., Romine, M. F., Shen, Y., Stritmatter, E., Tolic, N., Udseth, H. R., Venkateswaran, A., Wong, K.-K., Zhao, R., and Smith, R. D. (2002) Global analysis of the *Deinococcus radiodurans* proteome by using accurate mass tags. *Proc. Natl. Acad. Sci. U.S.A. 99*, 11049–11054.
67. Milton, K. W. (1994) DNA repair in the extremely radioresistant bacterium *Deinococcus radiodurans*. *Mol. Microbiol. 13*, 9–15.

BI800099D